AIAA JOURNAL
Vol. 33, No. 6, June 1995

Spray Impingement on a Hot Surface in Reacting Stagnation Flows

S. C. Li,* P. A. Libby,† and F. A. Williams‡
University of California, San Diego, La Jolla, California 92093-0411

This paper reports experimental and theoretical results concerning spray impingement on a hot wall in a laminar stagnating flow, both with and without a flat premixed flame present near the solid surface. Water droplets with diameters up to 200 μm are transported in a fuel-lean methane-air stream from a circular duct toward a stainless-steel plate. When the flame is present, it heats the wall to a temperature around 1250 K and causes the smaller droplets to disappear whereas the larger droplets cross the flame and impinge on the hot wall. Influences of the wall temperature on droplet impingement are studied by extinguishing the flame and allowing the plate to cool gradually to room temperature. Trajectories of the water droplets in the spray, illuminated by a Ar^+ laser, are recorded by a camera. Measurements of droplet diameter and of two components of velocity are made by a phase Doppler particle analyzer. Velocity profiles of the gas without spray are also measured with the phase Doppler particle analyzer by seeding the flow with MgO particles. The experimental results provide fundamental information on droplet vaporization in the flame, on the relationship between arrival and departure velocities of droplets striking the wall, and on the influence of wall temperature on droplet breakup. Simple theoretical models are developed to describe droplet collision dynamics at the wall and droplet trajectories in the stagnation flow. Comparisons between theory and experiment reveal how droplets respond to the flame and to the hot wall.

Nomenclature

B = transfer number, $c_p(T - T_p)/L$
C_D = drag coefficient, $24(1 + Re^{2/3}/6)/Re$
c_p = gas specific heat at constant pressure
D = dimensionless droplet diameter, D_p/D_{p0}
D_p = droplet diameter
D_{pA} = droplet arrival diameter before the collision
D_{pB} = droplet departure diameter after the collision
D_{p0} = droplet diameter at $\zeta = 0$
L = heat of vaporization
L_s = separation distance between the duct exit and the stagnation plate
Re = Reynolds number based on droplet diameter and relative velocity, $\sqrt{(u - u_p)^2 + (w - w_p)^2}(D_p W_0/\nu)$
Re_A = droplet arrival Reynolds number, $D_{pA}W_{pA}/\nu_p$
r = radial coordinate
T = gas temperature
T_p = droplet temperature
T_s = surface temperature of the impinging plate
t = time
U = gas radial velocity
U_p = droplet radial velocity
u = normalized gas radial velocity, U/W_0
u_p = normalized droplet radial velocity, U_p/W_0
W = gas axial velocity
W_p = droplet axial velocity
W_{pA} = droplet arrival velocity perpendicular to the wall
W_{pB} = droplet departure velocity perpendicular to the wall
W_0 = the axial exit velocity of the gas
We_A = droplet arrival Weber number, $\rho_p W_{pA}^2 D_{pA}/\sigma$
We_B = droplet departure Weber number, $\rho_p W_{pB}^2 D_{pB}/\sigma$
w = normalized gas axial velocity, W/W_0
w_p = normalized droplet axial velocity, W_p/W_0
Z_A = Ohnesorge number, $\sqrt{We_A}/Re_A = \sqrt{\nu_p^2 \rho_p/\sigma D_{pA}}$
z = axial coordinate
α = gas thermal diffusivity
β = dimensionless drag parameter, Eq. (19)
ε = vapor cushion thickness, Eq. (3)
ζ = dimensionless axial coordinate, z/L_s
ν = gas kinematic viscosity
ν_p = liquid kinematic viscosity
ξ = dimensionless radial coordinate, r/L_s
ρ = gas density
ρ_p = droplet liquid density
σ = surface tension of the liquid
τ = dimensionless time, $W_0 t/L_s$
τ_I = droplet residence time during collision

Introduction

SPRAY impingement on a solid surface is employed in many practical applications. Fire suppression by sprays impinging on burning surfaces is one of the examples that can be seen in daily life. Spray combustion in a confined chamber often involves impingement of the spray on solid surfaces. The influences of the gaseous flowfield on droplet dynamics, of the flame reaction zone on spray structure, and of droplet motion and breakup on droplet vaporization near hot surfaces are of fundamental importance and need attention that may ultimately lead to more efficient fire extinguishment and to improved performance of practical combustors such as furnaces, turbine combustors, diesel engines, and liquid rockets.

There have been many studies in which measurements are carried out on single droplets larger than 1 mm in diameter, individually falling upon a solid surface at temperatures between 300 K and 700 K. Relevant literature is reviewed by Wachters et al.,[1] by Wachters and Westerling,[2] and by Chandra and Avedisian[3]; some studies go back more than 100 years. A few studies have been reported on the impingement of sprays on solid surfaces. Fujimoto et al.[4] conducted a study of a diesel spray impinging on a flat plate at room temperature and found that the droplet number density becomes higher in the neighborhood of the stagnation plate and that there is a liquid film formed on the plate. Özdemir and Whitelaw[5,6]

Presented as Paper 94-3281 at the AIAA/ASME/SAE/ASEE 30th Joint Propulsion Conference, Indianapolis, IN, June 27–29, 1994; received July 14, 1994; revision received Dec. 2, 1994; accepted for publication Dec. 22, 1994. Copyright © 1995 by the American Institute of Aeronautics and Astronautics, Inc. All rights reserved.

*Research Scientist, Center for Energy and Combustion Research, Department of Applied Mechanics and Engineering Sciences. Member AIAA.
†Professor of Fluid Mechanics, Center for Energy and Combustion Research, Department of Applied Mechanics and Engineering Sciences. Fellow AIAA.
‡Professor of Engineering Physics and Combustion, Center for Energy and Combustion Research, Department of Applied Mechanics and Engineering Sciences. Fellow AIAA.

studied impingement of two-phase freejets on unheated and heated plates, and their results suggested that the secondary atomization with direct wall contact is the dominant process for the generation of a new size class of droplets. The single-droplet experiments provide useful information on collision and deformation of droplets interacting with plates. However, questions remain concerning the extent to which these results for larger droplets can be applied to smaller droplets (diameters less than 100 μm) in sprays of greater practical interest. An objective of the present work is to establish relationships between the hot-surface impingement behavior of large single droplets and small droplets in sprays with and without the flame present.

Because of the lack of knowledge on impingement dynamics, current theoretical models of diesel engines and liquid rockets often assume that the collision between each droplet and the wall is elastic. For example, Carpenter and Ramos[7] assume that droplets are reflected specularly at the piston in diesel engines. In studying liquid rockets, Larosiliere and Jeng[8] assume that the droplets either rebound or leave tangent to the wall depending on their Weber number. The present work shows that these assumptions are inaccurate and provides better approximations.

To improve our understanding of the detailed collision dynamics and to provide basic data for modeling involving droplet impingement on walls, the present study concentrates on spray structure in a well-defined stagnation flow. In this configuration droplet diameters range from 1 to 200 μm, and the surface temperature of the plate ranges up to 1250 K. We, thus, cover conditions relevant to many spray applications. A phase Doppler particle anaylzer (PDPA) is used to measure velocities and sizes of droplets at various positions on the axis so that the details of droplet response to the flame and to the hot plate can be characterized, and theoretical models of droplet collision with the wall and of droplet trajectory are developed to aid in interpretation of the experimental results.

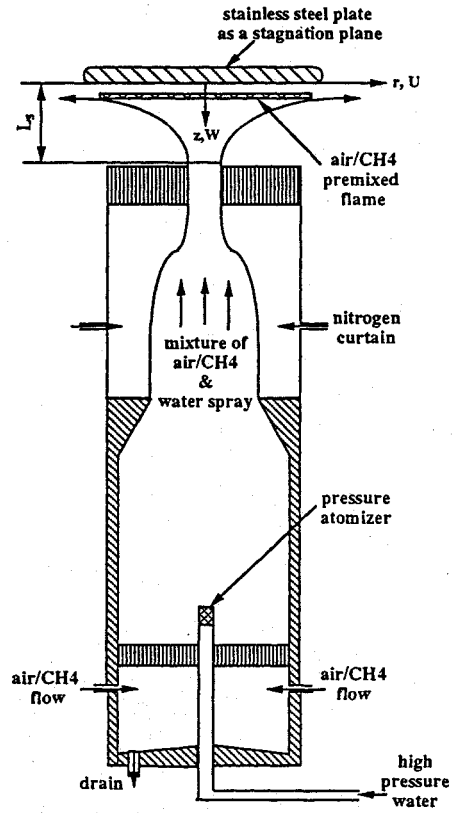

Fig. 1 Schematic diagram of the stagnation-flow burner for studying spray impingement on a hot wall.

Experiment Arrangement, Procedure, and Diagnostics

The experiment, as shown in Fig. 1, involves an axisymmetric duct with an exit radius of $R = 22.5$ mm and with its axis orthogonal to a stagnation plate made of stainless steel. The separation of the exit plane from the plate is $L_s = 30$ mm. The water sprays are carried by a methane-air gas mixture with an equivalence ratio of 0.9 flowing in a contoured tube. After exiting the duct, the spray stream flows upward and impinges on the stagnation plate. The water spray is produced by a pressure atomizer. The maximum diameter of the droplets that reach the plate is about 200 μm, but the probability of finding droplets with diameters ranging 110–200 μm is small, so that attention is focused here entirely on droplets with diameters between 1 and 110 μm. To have droplets with high enough kinetic energy to impinge on the stagnation plate, a relatively high flow rate is set, such that an exit axial velocity of $W_0 \approx 300$ cm/s for both gas and droplets is obtained. In this case, the arrival Weber number in the neighborhood of the stagnation plane before the collision with the wall is about 7 for a water droplet with diameter around 100 μm.

To initiate an experiment, the gas flow rate is first established. On igniting the stream with a torch a stable premixed flame is formed, and the surface temperature T_s of the stainless-steel plate, monitored by a pyrometer, begins to rise. After T_s becomes constant at approximately 1250 K, a valve from the high-pressure water tank to the atomizer is opened to form the spray. Since, contrary to some earlier experiments,[6] the droplet number density is very low ($<1/\text{mm}^3$), the spray is very dilute, and the influence of droplet cooling on the surface temperature is negligible when the flame is present. After steady-state conditions are established with the flame and the spray, PDPA data are collected at a selected position. The flame is then extinguished by momentarily reducing the methane flow rate by about 10% and then subjecting the flame to a puff of air. Subsequent PDPA samples are then acquired as the plate cools by radiation and convection in the stagnation flow at the same exit conditions that had been established with the flame.

The pyrometer (Pyro Micro-Optical Pyrometer) with a red filter responding to wavelengths around 0.65 μm is employed to measure the plate surface temperature. It is estimated that the error in its measurement is ± 50 K above 1000 K. Its reading was not affected by the thin blue flame, but because of its wavelength range it cannot measure temperatures below 1000 K. In view of this deficiency and the experimental difficulties in obtaining accurate thermocouple measurements of the surface temperature in the presence of the spray, T_s as a function of time t is obtained theoretically[9] from the heat-conduction solution

$$T_s = T_g + (T_{s0} - T_g)\left[\sum_{n=1}^{\infty} \frac{2\ell}{\ell(\ell+1)+\alpha_n^2} e^{-\alpha_n^2 t/t_s}\right] \quad (1)$$

where $T_g = 300$ K is the gas flow temperature without the flame, $T_{s0} = 1250$ K is the initial surface temperature, and t_s is the characteristic heat-conduction time. In Eq. (1), α_n, $n = 1, 2, \ldots$, are the positive roots of $\alpha \tan(\alpha) = \ell$. With the selections $\ell = 0.718$ and $t_s = 320$ s, results of the surface temperature measurements are consistent with Eq. (1) for $0 < t < 50$ s corresponding to T_s between about 1000 and 1250 K. This observation provides confidence in the procedure, even though the plate is not exactly semi-infinite. It is found from Eq. (1) that it takes 300 s for the surface temperature T_s to decrease from 1250 to 590 K after the flame is extinguished. Since droplet residence times in the stagnation flow are on the order of 10^{-2}s, the cooling rate can be neglected in describing droplet interactions. The experimental procedure, thus, is a convenient way to provide quasisteady conditions over a range of plate temperatures.

The PDPA that has been discussed in our previous work[10–12] is employed to study the spray structure. The probe volume formed by the laser beams of the PDPA is positioned at the desired point by moving the burner assembly axially and radially. Data on the arrival time (for determining the plate temperature), axial velocity, radial velocity, and diameter of droplets passing through the probe volume are then recorded by collecting 2000 samples at each probe position over a period up to 17 min (depending on the probe volume location) of steady-state conditions while the flame is present. Data without the flame are taken over the period of 300 s starting immediately after the flame is extinguished. Therefore, at the same position, the PDPA takes two sets of data: The first set is with the flame and at a plate surface temperature around 1250 K; the second set without the flame for a surface temperature decreasing from 1250 to 600 K.

This procedure is repeated until the desired survey of the flowfield of interest is completed.

After colliding on the wall, droplets become nonspherical but they recover their spherical shape after several periods of free oscillation. Since the vibration period of a freely oscillating droplet is very short for droplets smaller than 100 μm as shown in Eq. (2), we estimate that the nonspherical droplets are always confined in a region narrower than 1 mm adjacent to the wall. In the present experiment, all measurements are performed beyond this region so that the influence of nonsphericity of rebounding droplets on the measurement of the PDPA is negligible.

To observe droplets impinging on the hot plate and bouncing back, a thin laser sheet is constructed by directing a 2-W Ar^+-laser beam (wavelength 488 nm) through cylindrical lenses. Trajectories of the water droplets in the spray stream, illuminated by the laser sheet, are recorded by a camera. These photographs provide useful information in interpreting the experimental results obtained by the PDPA.

Gas velocity profiles in the stagnation flow must be known for interpreting droplet behaviors. Therefore, the gas streams without the spray are seeded with MgO particles of diameters smaller than 1 μm, and the PDPA is used as a laser Doppler velocimeter to measure the axial and radial velocity components form the exit plane to the wall. At each measuring location along the axis approximately 3000 pairs of velocity samples are collected and stored on disk for subsequent processing.[13]

Gas Velocity Profiles

The distribution of the normalized axial velocity w is shown in Fig. 2, where the open symbols apply for the stream with the flame and the closed symbols for the stream without the flame. The well-known nonmonotinicity of the profile with the flame[14] is evident and shows that the flame is located in the narrow region between $\zeta = 0.12$ and $\zeta = 0.18$ where the gas temperature is approximately equal to 2100 K. There will be a narrow boundary layer at the wall, estimated to extend from $\zeta = 0$ to $\zeta = 0.02$ under the present experimental conditions, where the temperature rapidly decreases to 1250 K. Similar velocity profiles were obtained in a previous study[13] on turbulent flow where the flame brush is thicker than the present flame.

The flow in the current experiment with the flame present is quite similar to the counterflows with symmetric back-to-back flames, analyzed by Libby and Williams.[15] With the temperature changes across the boundary layer on the plate neglected, the only difference is that the zero-gradient boundary condition for the radial velocity at the plane of symmetry must be replaced by a condition of zero radial velocity at the plate. It is, therefore, convenient to use the same formulation[15] here and to introduce the displacement correction of Kim et al.[16] for the flame, with Prandtl and Lewis numbers unity and plug-flow boundary conditions. An analysis by asymptotic methods paralleling that of Kim et al.[16] may then be performed (with the parameter[16] $\Gamma_\infty = -14.6$ for the present experiment with the flame and -0.9 without) resulting in profiles of the velocity components W, U, and gas temperature T. In the computation, the flame sheet is fixed at $\zeta = 0.135$, chosen to agree best with the experiment.

The predicted velocity distributions on the axis ($\xi = 0$) are plotted in Fig. 2. It can be seen that very good agreement between theory and experiment is achieved everywhere except in the narrow reaction zone. The predicted sharp change of the velocity in the flame is associated with use of the flame-sheet model of chemical behavior.[16] The comparison also indicates that the plug-flow boundary condition is a very good assumption in the present experiments. These results provide the gas-flow description needed for analyzing the droplet motion.

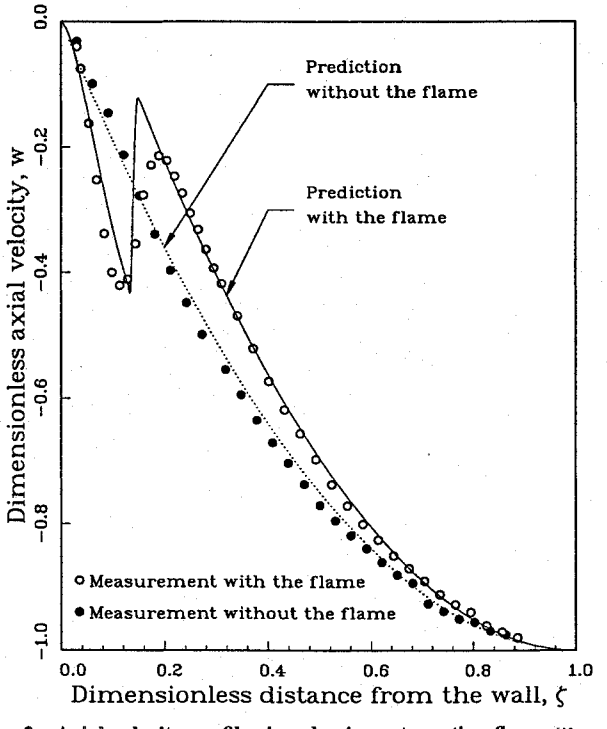

Fig. 2 Axial velocity profiles in a laminar stagnation flow with and without a premixed flame.

Experimental Results on Spray Structures

Photographs of water spray impingement on the hot surface in a stagnation flow with and without a flame are shown in Figs. 3a and 3b, respectively. The droplets are illuminated by the blue laser sheet. These photographs clearly show droplet trajectories that strike the red-hot wall, bounce back, and move up again. Figure 3a also shows that fewer droplets bounce back when the flame is present near the wall.

Figures 4 and 5 show typical PDPA results for the correlations of axial velocity with droplet diameter at various axial stations. In the present coordinate system as shown in Fig. 1, droplets moving toward the wall have negative axial velocities whereas those moving away from the wall have positive axial velocities. Our analyses of droplet behavior are based on these data. Data obtained with the flame are plotted in Fig. 4a whereas data at nearly the same wall temperature without the flame are shown in Fig. 4b. Each subfigure in Fig. 4b plots about 500 data points which were taken within 100 s starting immediately after the flame was extinguished. Figures 4a and 4b are put side by side for comparison.

The bottom plot in each figure shows that, under these experimental conditions, all droplets leave the duct exit with an upward velocity of about 300 cm/s, independent of their diameter, and these exit conditions are unaffected by the presence of the flame. The

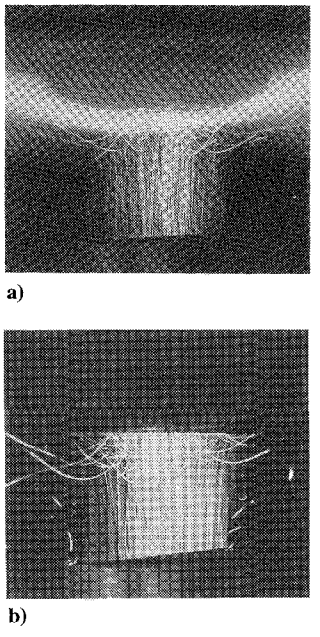

Fig. 3 Photographs of spray impingement on a hot surface in a stagnation flow: a) with a flame and b) without a flame.

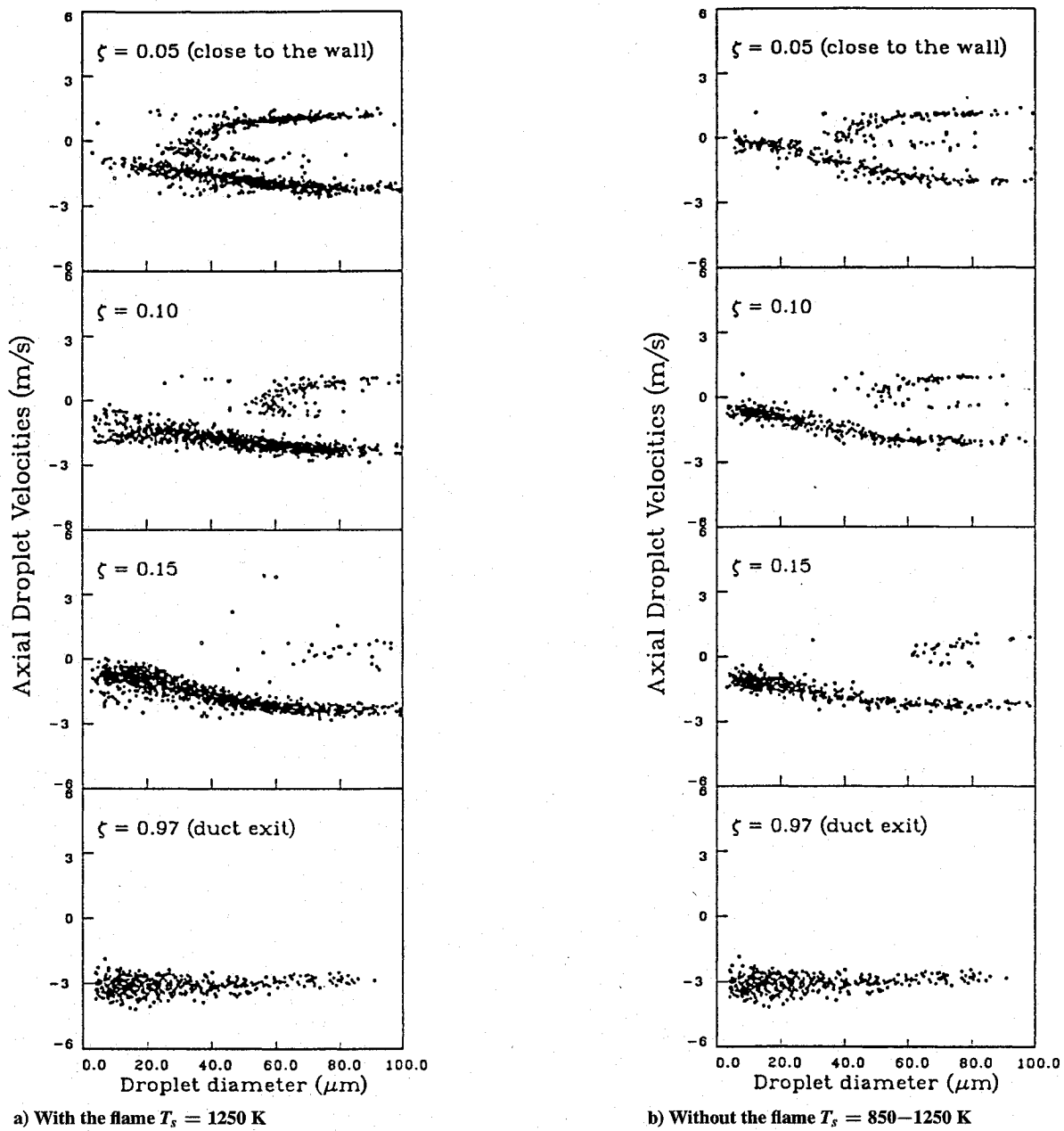

a) With the flame $T_s = 1250$ K

b) Without the flame $T_s = 850-1250$ K

Fig. 4 Correlation plots of axial velocity with droplet size at various axial positions.

second plot from the bottom shows that, again in both cases, as the droplets approach the stagnation plate, the smaller ones decelerate to a significantly lower velocity than the larger ones, that is, the larger droplets lag the gas flow and maintain a higher upward velocity toward the plate. A few scatter points in these two plots at axial velocities near zero and positive (downward) indicate that droplets bouncing back from the plate are beginning to be seen at $\zeta = 0.15$. The most remarkable results in Fig. 4 are, however, those in the top two plots for both cases. Qualitatively, there is not much difference even between the top two plots in Figs. 4a and 4b, thereby indicating that, at a given surface temperature, the presence of the flame has little effect on velocity distributions of droplets that have interacted with the wall (the flame does promote vaporization and, thereby, gives a much lower number density and a larger proportion of larger droplets, as reported more quantitatively later). The most dominant feature of these top two plots is the clearly trimodal velocity distributions of the larger droplets. In addition to the incident group with the larger upward velocity, there is a less populated reflected group having a downward velocity and a least populated turnaround group showing a small upward velocity. These last two groups meet at a droplet diameter seen most clearly from the top three plots in Fig. 4b to increase with increasing distance from the wall. Thus, a C-shaped curve is discernible in Fig. 4, above the base (incident) curve, leaving essentially no small droplets in the second and third branches. It is the quantitative explanation of these features that provide the most important information concerning droplet-wall interactions.

The flame causes most of the small droplets to vaporize before reaching the plate. For instance, D_{10}, the arithmetic mean diameter at $\zeta = 0.05$ on the stagnation streamline with the flame present, is about 52 μm, whereas $D_{10} = 25$ μm at the same position without the flame. The number density n in the neighborhood of the stagnation plane with the flame is much lower than that without the flame. For example, $n = 25$ cm^{-3} at $\zeta = 0.05$ with the flame, whereas $n = 250$ cm^{-3} at the same position without the flame. Because of the droplets bouncing back, the droplet number density in the neighborhood of the stagnation plate without a flame present is about two to three times higher than that at the exit in the present experiment.

The data in Fig. 4 at $\zeta = 0.05$ provide the information needed for analyzing the collisions of droplets with the hot surface. Because of short residence time, changes in velocities and diameters of most droplets between $\zeta = 0$ and $\zeta = 0.05$ can be neglected, so that incident and reflected droplet velocities can be approximated as those seen in the top plots in Fig. 4. The arrival velocity (the incident velocity) W_{pA}, just before the impact, can be found in the bottom

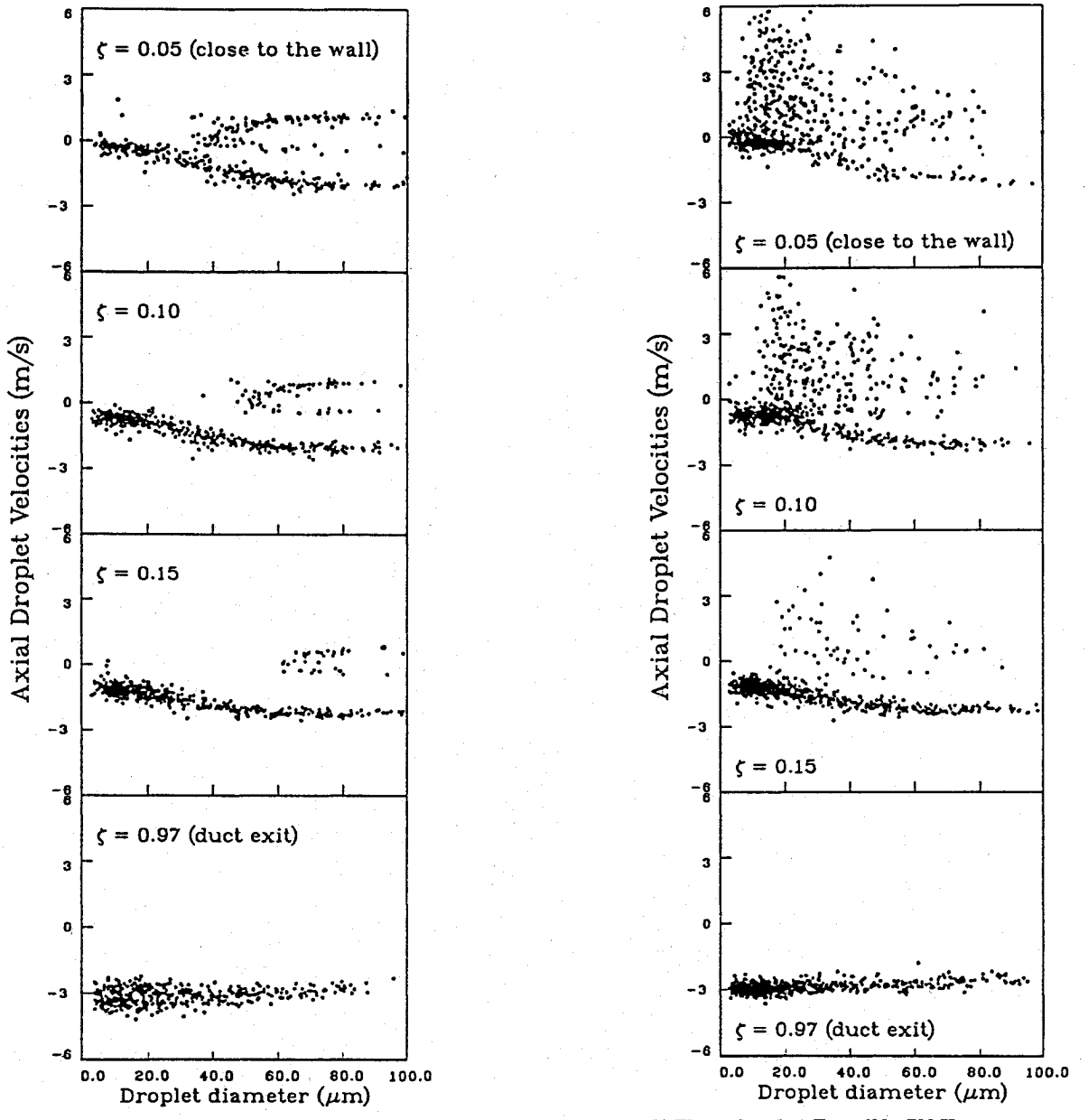

a) The hotter plate $T_s = 800-1000$ K

b) The cooler plate $T_s = 600-700$ K

Fig. 5 Correlation plots of axial velocity with droplet size at various axial positions without the flame.

branch whereas the departure velocity (the reflected velocity) W_{pB}, just after collision, appears in the top branch. The velocity magnitude of both arrival and departure can be seen to increase slightly with droplet diameter and, therefore, the larger droplets have higher kinetic energies and larger Weber numbers before and after the impingement. These experimental results can be used to estimate how much kinetic energy is dissipated at the wall during impingement, as discussed in the next section.

Figure 5 shows the effect of the plate temperature on the interaction of the droplets with the hot surface. Figure 5a plots the data taken from $t = 30$ to 130 s after flame extinguishment, data which correspond to $T_s = 800$–1000 K, whereas Fig. 5b plots data taken from $t = 250$ to 280 s, data which correspond to $T_s = 600$–700 K. The results in Fig. 5a are quite similar to those in Fig. 4b, as expected, but comparison of Figs. 5a and 5b shows that at plate temperatures below about 700 K, the droplets interact with the surface in a very different manner. The distribution of incident droplets (moving upward) in Fig. 5b is essentially the same as in Fig. 5a, but droplets that bounce back (those with positive velocity) behave quite differently. There is a large number of smaller droplets bouncing back, the distinctively trimodal velocity distributions is destroyed, and the velocity spread is greatly increased with downward velocities of droplets with diameters around 20 μm reaching more than 600 cm/s, three times higher than the maximum impinging velocity.

It is noteworthy that this altered behavior is entirely consistent with observations made on individual larger droplets,[1–3] which have been explained by reduced vaporization rates of incident droplets at lower plate temperatures allowing liquid to contact roughness peaks, thereby creating many nucleation of sites in the liquid which introduce bubbles that help to break up the liquid into smaller droplets and to propel these droplets away at higher velocities because of the increased rate of heat transfer associated with metal-liquid contact. This cooler-surface phenomenon is later excluded in our considerations of droplet-plate interaction, which is restricted to conditions leading to the trimodal velocity distributions.

Theoretical Consideration of Droplet Collision with the Hot Wall

On the basis of observations made in experiments on single droplets, we propose the simplified impingement model illustrated in Fig. 6. Before the collision, the droplet with diameter D_{pA} move vertically toward the wall at the arrival velocity W_{pA}. During impingement droplet behavior can be divided into two parts; an

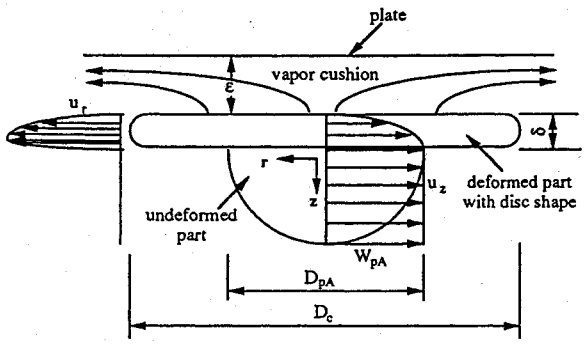

Fig. 6 Schematic diagram of a deformed droplet during impingement on a very hot wall.

undeformed part in which there are no velocity gradients and a disk with a diameter D_c and thickness δ. Because of the high surface temperature, there is a vapor cushion of thickness ε between the disk and wall. Since ε is small compared with D_c, we only need to consider the radial momentum equation in which the pressure gradient is balanced by the shear stress. Representative velocity profiles in the liquid are sketched qualitatively in Fig. 6.

In earlier works[1,2] theoretical estimates have been given for ε, for the interaction period τ_I between the droplet and the surface, and for the volume change of the droplet through vaporization during interaction. The resulting formulas[2] are applied here to the droplets in the present experiments. Thus, the interaction time is approximated as the fundamental oscillation period of the droplet:

$$\tau_I = \frac{\pi}{4}\sqrt{\frac{\rho_p D_{pA}^3}{\sigma}} \tag{2}$$

with the density ρ_p and surface tension evaluated at room temperature, giving values which differ by less than 10% from those evaluated at the normal boiling point. Equation (2) gives $\tau_I = 10$ ms for $D_{pA} = 2.3$ mm but $\tau_I \approx 0.1$ ms for $D_{pA} = 100$ μm, indicating that the interaction times for the small droplets in the present study are extremely short.

The droplet deceleration during interaction is approximated here as W_{pA}/τ_I. Since this is very large compared with the normal acceleration of gravity, the gravitational acceleration, included in the theoretical formulas,[2] is neglected here. From experiment,[3] the maximum value of D_c is roughly approximated as $2.3D_{pA}$. The formulas[2] then provide the estimates

$$\frac{\varepsilon}{D_{pA}} = \frac{1.13}{D_{pA}^{0.125}}\left[\left(\frac{T_s + T_p}{T_p}\right)^3 \frac{\rho\alpha B}{\sqrt{\rho_p\sigma}} \frac{\nu}{D_{pA}W_{pA}}\right]^{0.25} \tag{3}$$

for the relative cushion thickness of the vapor layer, and

$$\frac{\Delta V}{V_A} = \frac{2.8}{D_{pA}^{0.375}}\left(\frac{\rho\alpha B}{\sqrt{\rho_p\sigma}}\right)^{0.75}\left(\frac{T_s + T_p}{T_p}\frac{D_{pA}W_{pA}}{\nu}\right)^{0.25} \tag{4}$$

for the factional volume decrease during interaction. Here the transfer number is $B = c_p(T_s - T_p)/L$. For water droplets with $\sigma = 72$ dyne/cm, $\rho_p = 1$ mg/cm^3, $\rho = 1 \times 10^{-3}$ g/cm^3, $\alpha = \nu = 0.15$ cm^2, $B = 0.41$, $T_s = 1250$ K, $T_p = 373$ K, and $W_{pA} = 200$ cm/s, it is found from Eqs. (3) and (4) that as droplet diameter decreases from 200 to 30 μm the maximum value of $\Delta V/V_A$ increases from 0.6 to 0.7% and of ε/D_{pA} from 13% to 26%. Here we see that the cushion thickness is around 15 μm for the conditions just cited. Noting that

$$\frac{D_{pB}}{D_{pA}} = \left(1 - \frac{\Delta V}{V_A}\right)^{\frac{1}{3}} \tag{5}$$

we conclude that the diameter change is less than 1% during interaction with the wall and can be neglected, as would be expected from the very small value of τ_I.

Figure 4 shows clearly that the magnitude of the velocity of the reflected droplet is less than that of the incident droplet. This implies that the collision is not elastic and that energy must be dissipated during the interaction with the wall. For the model illustrated in Fig. 6, this loss must result from viscous dissipation in the flow in the liquid disk. It is of interest to attempt to estimate this dissipation, so that improved descriptions of results of spray interactions with hot walls can be obtained. The relationship between the arrival kinetic energy, defined as $E_{kA} = (\pi/12)\rho_p D_{pA}^3 W_{pA}^2$, and the departure kinetic energy, defined as $E_{kB} = (\pi/12)\rho_p D_{pB}^3 W_{pB}^2$ can be written as

$$E_{kA} - E_{kB} = E_d \tag{6}$$

where E_d, the energy dissipated in deforming droplet against viscosity, is given by

$$E_d \approx \int_0^{\tau_I}\int_V \rho_p \nu_p \left(\frac{\partial u_i}{\partial x_j} + \frac{\partial u_j}{\partial x_i}\right)\frac{\partial u_i}{\partial x_j} \mathrm{d}V\mathrm{d}t \tag{7}$$

Noting that velocity gradients $\partial u_r/\partial z$ and $\partial u_z/\partial z$ are dominant in the disk as shown in Fig. 6 and that the maximum velocity magnitudes in both the z and r directions are approximately[17] W_{pA}, we obtain the estimate

$$\left(\frac{\partial u_i}{\partial x_j} + \frac{\partial u_j}{\partial x_i}\right)\frac{\partial u_i}{\partial x_j} \approx \frac{W_{pA}}{\delta}\frac{W_{pA}}{\delta} \tag{8}$$

As a first approximation we further assume that δ and ν_p are independent of time and position, so that we have

$$E_d \approx \rho_p \nu_p (W_{pA}/\delta)^2 \left(\pi/4D_c^2\delta\right)\tau_I \tag{9}$$

where D_c is now the average disk diameter. With δ approximated from boundary-layer considerations as

$$\delta \approx \sqrt{\nu_p D_{pA}/W_{pA}} \tag{10}$$

we find that if the simple estimate $D_c \sim D_{pA}$ is employed, then it is not possible to fit the data in Fig. 4 on the relationship between W_{pB} and W_{pA} for all of the different droplet diameters. Since it is a balance between surface tension and viscosity that determines the growth of the disk, it is reasonable to assume that

$$D_c \sim D_{pA} Z_A^{\gamma} \tag{11}$$

where the exponent γ of the Ohnesorge number is considered to be a constant to be determined empirically. Since an increase in surface tension should decrease D_c, we anticipate that $\gamma > 0$. Within the context of the present model, available data are correlated best by $\gamma = 0.25$; correlations are quite poor for $\gamma = 0.2$ or for $\gamma = 0.3$. With this value of γ, Eq. (9) becomes

$$E_d = C E_{kA} We_A^{0.25} Z_A \tag{12}$$

where C is a constant.

Equation (12) indicates that the dissipated energy increases with increasing Weber number of the incident droplet and is inversely proportional to the drop arrival Reynolds number. By substituting Eq. (12) into Eq. (6), the departure velocity is found to be

$$W_{pB} = W_{pA}\sqrt{1 - CWe_A^{0.25} Z_A} \tag{13}$$

whereas the departure Weber number can be written as

$$We_B = We_A\left(1 - CWe_A^{0.25} Z_A\right) \tag{14}$$

where droplet diameter is assumed to be unchanged during the collision as discussed earlier. Thus, the change in Weber number is due to the change in kinetic energies before and after collision. From Eq. (13) we find that the ratio of the departure velocity to the arrival velocity decreases with increasing We_A and Z_A.

Figures 7 and 8 show the comparisons between experiment and prediction according to Eq. (14). The data taken after flame extinguishment, with $T_s = 1000$–1250 K are shown in Fig. 7, and those with the flame are shown in Fig. 8. The dependence of W_{pA} and W_{pB} on D_{pA} are taken from the lower and upper branches, respectively,

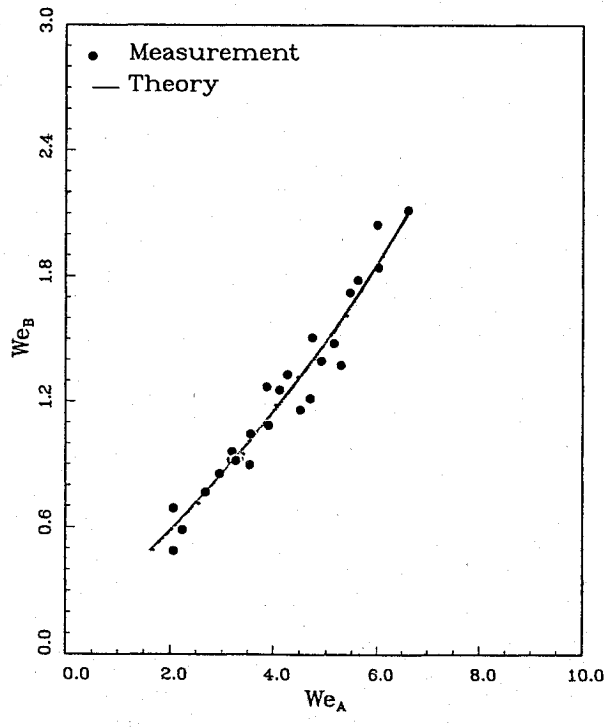

Fig. 7 Comparison between theory and experiment concerning droplet Weber numbers before and after collision with the hot wall in a stagnation stream without a flame.

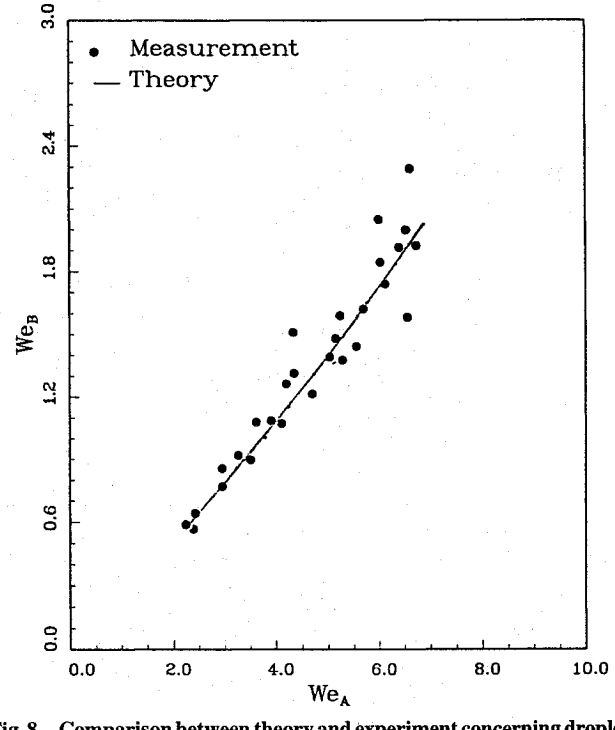

Fig. 8 Comparison between theory and experiment concerning droplet Weber numbers before and after collision with the hot wall in a stagnation stream with a flame.

of the data at $\zeta = 0.05$ in Fig. 4. In Figs. 7 and 8, the droplet diameter D_{pA} ranges from 30 to 100 μm, W_{pA} from 100 to 250 cm/s, and W_{pB} from 50 to 150 cm/s. Based on these measured velocities and droplet diameters, the arrival Weber number We_A is found to be in the range from 2 to 7 and the Ohnesorge number Z_A from 0.01 to 0.05; the departure Weber number We_B varies from 0.6 to 2.5. The value $C = 37$ is used here, and excellent agreement between the theory and experiment is then achieved in both Figs. 7 and 8 (where variations of We_{pA} from 2 to 7, and of Z_A from 0.01 to 0.05 were obtained from a smoothed curve through the bottom branch

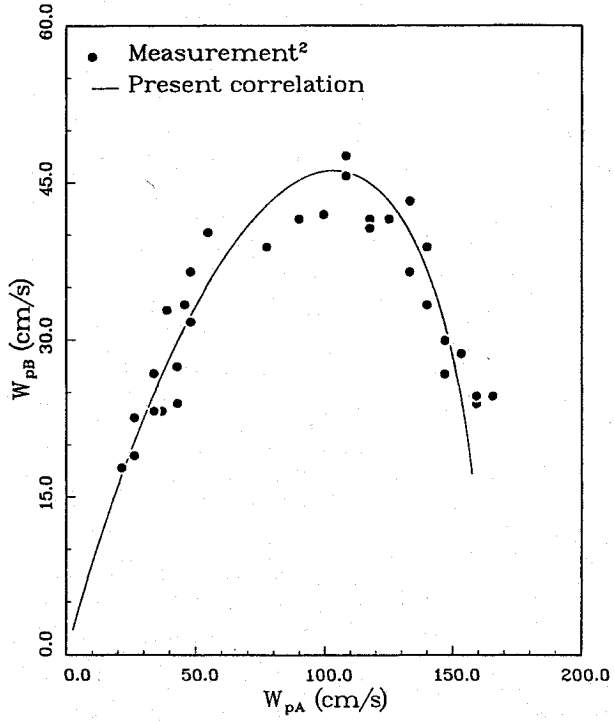

Fig. 9 Comparison between theory and experiment concerning departure velocity vs arrival velocity for a 2.3-mm water droplet impinging on a wall at temperature 700 K.

of the top plot of Fig. 4). It is found that departure velocity W_{pB} is roughly half of W_{pA}, which means a substantial amount of kinetic energy is dissipated during droplet collision.

As a further test of the correlation, it is of interest to see whether previous data on larger single droplets are consistent with Eq. (13) Figure 9 shows the departure velocity W_{pB} as a function of the incident velocity W_{pA} for water droplets of diameters of 2.3 mm, striking a polished gold plate with $T_s \approx 700$ K. The points are from experiment and the curve from Eq. (13) with $C = 135$, employing the room-temperature water values $\sigma = 70$ dyne/cm and $\nu_p = 0.01$ cm^2/s for evaluating We_A and Z_A. The agreement is excellent over a wide range of W_{pA}, and the correlation reproduces well the observed nonmonotonicity. The value of C here is more than four times that needed in Figs. 7 and 8, where the same values of ν_p and σ were employed. However, it may be expected that the smaller droplets are heated more quickly and that it may, therefore, be more approximate to employ values of σ and ν_p at the boiling point in Figs. 7 and 8. With these values, ($\sigma = 61$ dyne/cm and $\nu_p = 0.003$ cm^2/s), it is found that $C \approx 130$ is needed in Figs. 7 and 8. This value agrees well with that employed in Fig. 9.

Droplet Trajectories

Besides the droplet-plate interaction information on W_{pA} and W_{pB} as functions of D_p, Figs. 4 and 5a provide values of the droplet diameter at which the second and third branches meet, as a function of ζ. This function, or its inverse, the turnaround distance from the plate as a function of D_p, depends not only on the nature of the droplet-plate interaction but also on the trajectory of the droplet in the stagnation flow. It is, therefore, of interest to compute droplet trajectories and to calculate the turnaround distance from the results, for comparison with experiment.

The prediction of particle trajectories in stagnation-flow spray has been discussed in our previous work.[10–12] The axial velocity W_p and radial velocity U_p of a droplet are expressed in the form $W_p = W_0 w_p(\zeta)$, and $U_p = W_0 u_p(\zeta, \xi)$, respectively. When these forms are substituted into the equations of motion of a spherical droplet with diameter D_p, it is found that

$$\frac{dw_p}{d\tau} = -\frac{3w_p}{D}\frac{dD}{d\tau} + \beta f_d(w - w_p) \qquad (15)$$

$$\frac{du_p}{d\tau} = -\frac{3u_p}{D}\frac{dD}{d\tau} + \beta f_d(u - u_p) \tag{16}$$

$$\frac{d\zeta}{d\tau} = w_p \tag{17}$$

$$\frac{d\xi}{d\tau} = u_p \tag{18}$$

where

$$\beta = 18(\rho/\rho_p)\left(L_s\nu/W_0D_p^2\right) \qquad f_d = \left(1 + Re^{\frac{2}{3}}/6\right) \tag{19}$$

the symbols having been defined in the Nomenclature. Gravity is neglected because its contribution is less than 2% for the present experiments. In Eqs. (15) and (16), the mass-loss terms $dD/d\tau$ are small and can be neglected; they were not included in our earlier work. To evaluate $dD/d\tau$, we employ the formulas of Faeth[18]:

$$\frac{dD}{d\tau} = -\frac{2}{9} f_m \beta D \ell_n(1 + B) \tag{20}$$

where $f_m = 1 + 0.278\sqrt{Re}/\sqrt{1 + 1.232/Re}$, which is a correction for the relative motion between the droplet and gas.

The initial conditions at $\tau = 0$ for Eqs. (15–18) and Eq. (20) are

$$w_p = w_{p0}, \qquad u_p = u_{p0}, \qquad \zeta = 1, \qquad \xi = \xi_0, \qquad D = 1 \tag{21}$$

where the third and fourth conditions specify the position of the droplet, the first two give the droplet velocity at that position, and the last describes the droplet diameter. By solving Eqs. (15–18) and Eq. (20) numerically with initial conditions specified by Eq. (21), droplet trajectories in the ζ–ξ plane between $\zeta = 0$ and $\zeta = 1$ can be found. Solutions at $\zeta = 0$ provide droplet arrival velocity, diameter, and position at the wall, W_{pA}, U_{pA}, D_{pA}, and ξ_A, respectively.

From our previous results, droplet conditions after collision with the wall are given by

$$w_p = W_{pB}/W_0, \qquad u_p = U_{pA}/W_0, \qquad \zeta = 0$$
$$\xi = \xi_A, \qquad D = D_{pA}/D_{p0} \tag{22}$$

where it is assumed that the radial velocity components of droplets is unchanged after collision based on the experimental observation by Wachters and Westerling.[2] Droplet trajectories after collision can be obtained by solving the same set of differential equations with these new initial conditions. These initial parameters are all obtained from the analysis of the previous section. By repeating this procedure, the complete trajectory of any given droplet can be found in the ζ–ξ plane, and then comparisons between theory and experiment can be made.

Predicted trajectories of water droplets are shown in Figs. 10 and 11 where the dashed, chain dotted, and solid curves correspond to $D_{p0} = 5$, 65, and 110 μm. The initial conditions at $\tau = 0$ in both figures are $w_{p0} = 1$, $u_{p0} = 0$, $\zeta_0 = 1$, and $\xi_0 = 0.05$. In Fig. 11, the premixed flame is located at $\zeta \approx 0.15$. We see from this figure that droplets move upward from the exit plane and cross the flame; the smaller droplets then disappear through vaporization before striking the wall, but the larger droplets impinge on the wall. The computation indicates that droplets with diameter smaller than 25 μm vaporize completely before reaching the wall under the present flow conditions. On the other hand, larger droplets may collide with the hot wall twice before being vaporized completely or transported beyond the plate.

In Fig. 11, it is of interest to compare the trajectory of a 110-μm drop with that of a 65-μm droplet. The droplet of 110 μm strikes the wall at $\xi = 0.053$ with arrival velocity $W_{pA} = 254$ cm/s and departure velocity $W_{pB} = 140$ cm/s, whereas the 65-μm droplet collides with the wall at $\xi = 0.058$ with $W_{pA} = 207$ cm/s and $W_{pB} = 108$ cm/s. Since the 110-μm droplet has a higher departure velocity, it bounces back farther, exhibiting a turning point about 13 mm from the wall, much larger than the 3.8-mm distance for the 65-μm droplet. When the droplets move up again from the turning point to strike the wall a second time, the larger droplet strikes at

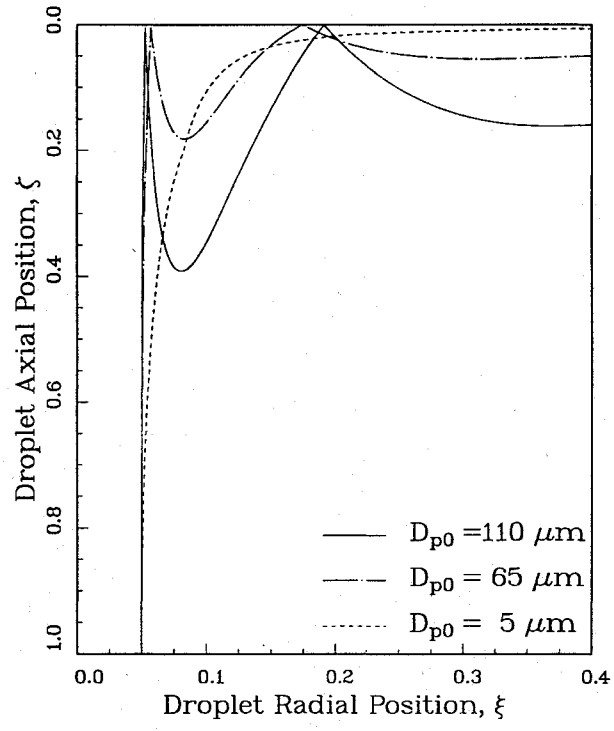

Fig. 10 Predicted trajectories of water droplets with different diameters in a stagnating stream with $T_s \approx 1000$ K and no flame.

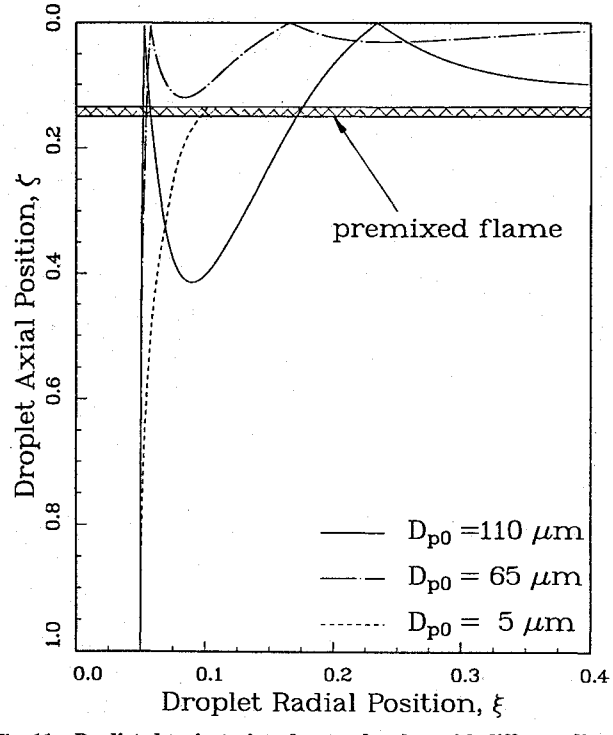

Fig. 11 Predicted trajectories of water droplets with different diameters in a stagnating stream with $T_s \approx 1250$ K and a flame present.

$\xi = 0.234$ with $W_{pA} = 56$ cm/s and $W_{pB} = 45$ cm/s whereas the smaller one hits at $\xi = 0.166$ with $W_{pA} = 52$ cm/s and $W_{pB} = 40$ cm/s. It can be seen that the arrival kinetic energies for each of these droplets at the second collision are much lower than those at the first collision. Therefore, the distance to the second turning point is very short for both of them. Here, we also see that the difference between the incident and reflected velocities becomes smaller at the second collision since the arrival velocity is low.

The results shown in Figs. 10 and 11 are quite similar except that in the cold-flow case of Fig. 10, which corresponds to Fig. 4b, droplet vaporization does not occur. Because of this difference, the

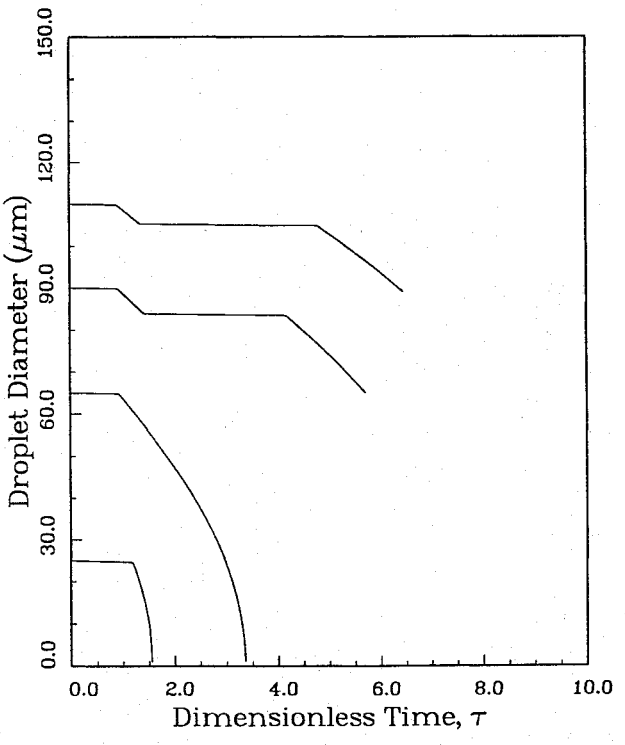

Fig. 12 Predicted droplet diameter vs time in a stagnating stream with $T_s \approx$ 1250 K and a flame present.

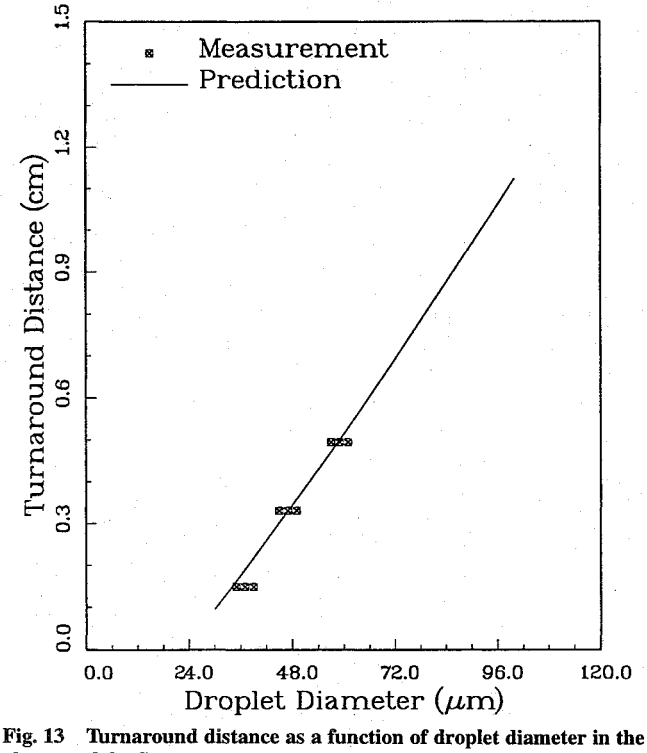

Fig. 13 Turnaround distance as a function of droplet diameter in the absence of the flame.

turnaround distances differ in the two figures. The 5-μm droplet in Fig. 10 essentially follows the gas and does not collide with the plate. In Fig. 11, this droplet barely survives its meeting with the flame, as may be seen more directly in the corresponding droplet diameter histories, plotted in Fig. 12. In that figure, the 65-μm droplet does not penetrate the flame a second time after bouncing, and it disappears at the edge of Fig. 11. The two larger droplets in Fig. 12 do penetrate the flame a second time and, therefore, experience a second vaporization-free period in the cold flow.

Figures 13 and 14 compare the observed and predicted turnaround distances. The theoretical calculations are made as described earlier whereas the experimental results correspond to intersection of the

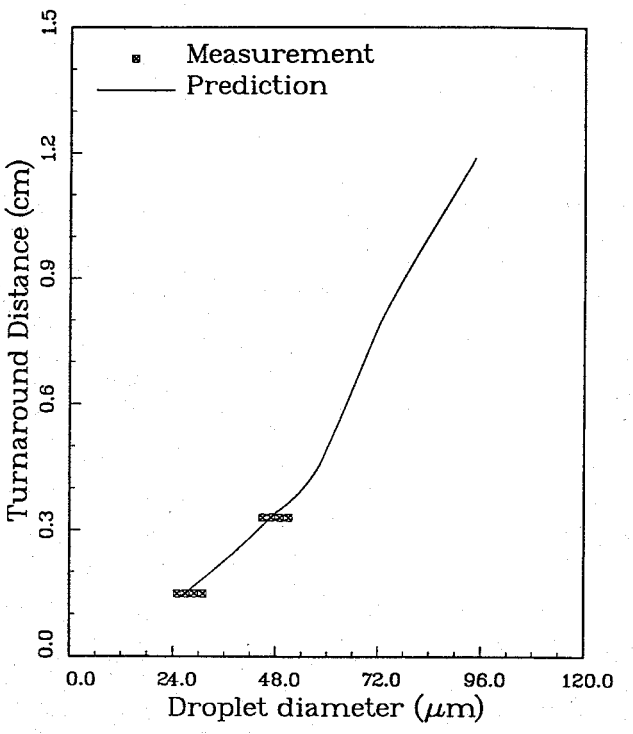

Fig. 14 Turnaround distance as a function of droplet diameter in the presence of the flame.

second and third branches of the C curves in Fig. 4. Since measurements were repeated several times at the same position, there are three or four data points at each turnaround distance. These figures show that the agreement between experiment and theory is good. There are no data points for diameter larger than 70 μm shown here because the probability of finding large droplets at farther turning points from the wall is extremely small. The turnaround distance in the stream without the flame (Fig. 13) increases approximately linearly with diameter, whereas that with flame present is nonlinear because of the influence of the flame. The droplet diameter in Fig. 14 is smaller than its initial value because of vaporization, and the small droplets become smaller more rapidly than the large ones, thereby producing the predicted nonlinearity.

Conclusion

The results of an experimental and theoretical study on spray impingement on a hot wall in stagnation flow with and without a flame are reported. Correlation plots of axial velocity with water drop size are obtained at various stations on the axis by PDPA. When the wall surface temperature is higher than 800 K, a trimodal distribution of droplets is seen in the neighborhood of the impingement plate. The structure of the trimodality in the flow with the flame is different than without the flame because of droplet vaporization. When the wall temperature is lower than 700 K, the trimodality disappears, and we observe a large number of small droplets randomly flying away from the wall at velocities much higher than the arrival velocity, as a consequence of shattering and rejection of droplets as they contact the hot wall and form high-pressure bubbles.

A simple theoretical model is suggested for describing droplet behavior during the collision. It is found that the droplet size change during the collision is negligibly small. The thickness of the cushion between droplet and the hot wall is found to increase with wall temperature and drop size but to decrease with increasing arrival velocity. The ratio of the departure to the arrival velocity decreases with increasing Ohnesorge number and Weber number of the droplet as long as the droplet does not break up. Since the departure velocity is smaller than the arrival velocity, the angle of incidence is greater than the angle of reflection during the collision and, consequently, successive branches of the trimodal velocity distribution are less populated.

This study shows that a fairly simple theory can produce good agreement with experimental observations on droplet impingement

on the wall. The droplet trajectory is influenced not only by the collision but also by the flame. Because of the flame, the droplet becomes smaller, and thus the relative velocity between the droplet and gas decreases. Improved descriptions for spray interactions at hot walls can be extracted from the results.

Acknowledgment

This research is supported by the Department of Energy, Office of Basic Energy Sciences, Division of Engineering and Geosciences, under Contract DE-F003-87ER13685.

References

[1]Wachters, L. H., Bonne, H., and Van Nouhuis, H. J., "The Heat Transfer from a Hot Horizontal Plate to Sessile Water Drops in the Spheroidal state," *Chemical Engineering Science*, Vol. 21, Oct. 1966, pp. 923–936.

[2]Wachters, L. H., and Westerling, N. A. J., "The Heat Transfer from a Hot Wall to Impinging Water Drops in the Spheroidal State," *Chemical Engineering Science*, Vol. 21, Nov. 1966, pp. 1047–1056.

[3]Chandra, S., and Avedisian, C. T., "On the Collision of a Droplet with a Solid Surface," *Proceedings of the Royal Society of London, Series A*, Vol. 432, No. 1884, 1991, pp. 13–41.

[4]Fujimoto, H., Minoura, A., Cho, I. Y., Saitou, M., and Senda, J., "Characteristics of a Diesel Spray Impinging on a Flat Plate," *Heat and Mass Transfer in Gasoline and Diesel Engines*, edited by D. B. Spalding and N. H. Afgan, Hemisphere, New York, 1989, pp. 291–303.

[5]Özdemir, İ. B., and Whitelaw, J. H., "Impingement of an Axisymmetric Jet on Unheated and Heated Flat Plates," *Journal of Fluid Mechanics*, Vol. 240, July 1992, pp. 503–532.

[6]Özdemir, İ. B., and Whitelaw, J. H., " Impingement of an Unsteady Two-Phase Jet on Unheated and Heated Flat Plates," *Journal of Fluid Mechanics*, Vol. 252, July 1993, pp. 499–523.

[7]Carpenter, M. H., and Ramos, J. I., "Spray Penetration, Vaporization, and Mixing in Diesel Engines," *Heat and Mass Transfer in Gasoline and Diesel Engines*, edited by D. B. Spalding and N. H. Afgan, Hemisphere, New York, 1989, pp. 201–214.

[8]Larosiliere, L. M., and Jeng, S. M., "Bipropellant Spray Combustion Modeling in Small Rocket Engines," AIAA Paper 91-2197, June 1991.

[9]Carslaw, H. S., and Jaeger, J. C., *Conduction of Heat in Solids*, 2nd ed., Oxford Univ. Press, Oxford, England, UK, 1959, pp. 114–132.

[10]Li, S. C., Libby, P. A., and Williams, F. A., "Spray Structure in Counterflowing Streams with and without a Flame," *Combustion and Flame*, Vol. 94, No. 1-2, 1993, pp. 161–177.

[11]Li, S. C., Libby, P. A., and Williams, F. A., "Droplet Relative Motion and Spray Structure in Counterflowing Streams," *Fluid Mechanics and Heat Transfer in Sprays*, edited by J. W. Hoyt, T. J. O'Hern, C. Presser, A. K. Gupta, and R. L. Alpert, American Society of Mechanical Engineers, New York, 1993, pp. 25–34.

[12]Li, S. C., Libby, P. A., and Williams, F. A., "Turbulent Sprays in Stagnation Flows," *Atomization and Sprays* (to be published).

[13]Li, S. C., Libby, P. A., and Williams, F. A., "Experimental Investigation of a Premixed Flame in an Impinging Turbulent Stream," *Twenty-Fifth Symposium (International) on Combustion*, Combustion Inst. (to be published).

[14]Daneshyar, H., Mendes-Lopes, J. M. C., and Ludford, G. S. S., "Effect of Strain Fields on Burning Rate," *Nineteenth Symposium (International) on Combustion*, Combustion Inst., Pittsburgh, PA, 1982, pp. 413–421.

[15]Libby, P. A., and Williams, F. A., "Strained Premixed Laminar Flames with two Reaction Zones," *Combustion Science and Technology*, Vol. 37, No. 5-6, 1984, pp. 221–252.

[16]Kim, J. S., Libby, P. A., and Williams, F. A., "On the Displacement Effects of Laminar Flames," *Combustion Science and Technology*, Vol. 87, No. 1-6, 1992, pp. 1–25.

[17]Harlow, F. H., and Shannon, J. P., "The Splash of a Liquid Drop," *Journal of Applied Physics*, Vol. 38, No. 10, 1967, pp. 3855–3866.

[18]Faeth, G. M., "Evaporation and Combustion of Sprays," *Progress in Energy and Combustion Science*, Vol. 9, No. 1-3, 1983, pp. 1–76.